



1 **A deep learning method for convective weather** 2 **forecasting : CNN-BiLSTM-AM (version 1.0)**

3 Jianbin Zhang^{1,3}, Zhiqiu Gao^{1,2}, Yubin Li¹, Yuncong Jiang¹

4 ¹ School of Atmospheric Physics, Nanjing University of Information Science & Technology, Nanjing,
5 210044, China

6 ² State Key Laboratory of Planetary boundary layer Physics and Atmospheric chemistry, Institute of
7 Atmospheric Physics, Chinese Academy of Sciences, Beijing,100081,China

8 ³ College of Artificial Intelligence, Henan University, Kaifeng, 475000, China

9 *Correspondence to:* Dr. Zhiqiu Gao (zgao@nuist.edu.cn) and Dr. Yubin Li (liyubin@nuist.edu.cn)

10 **Abstract.**This work developed a CNN-BiLSTM-AM model for convective weather forecasting using
11 deep learning algorithms based on reanalysis and forecast data from the NCEP GFS, the performance of
12 the model was evaluated. The results show that: (1) Compared to traditional machine learning algorithms,
13 the CNN-BiLSTM-AM model has the ability to automatically learn deeper nonlinear features of
14 convective weather. As a result, it exhibits higher forecasting accuracy on the convective weather dataset.
15 Furthermore, as the forecast lead time increases, the information value provided by this model also
16 changes. (2) In comparison to subjective forecasts by forecasters, the objective forecasting approach of
17 the CNN-BiLSTM-AM model demonstrates advantages in metrics such as Probability of Detection
18 (POD), False Alarm Rate (FAR), Threat Score (TS), and Missing Alarm Rate (MAR). Specifically, the
19 average TS score for heavy precipitation reaches 0.336, which is a 33.2% improvement compared to the
20 forecaster's score of 0.252. Moreover, due to the CNN-BiLSTM-AM model's ability to automatically
21 extract classification features based on a large sample dataset and consider a comprehensive range of
22 convective parameters, it effectively reduces the FAR. (3) The interpretability study of the machine
23 learning-based convective weather mechanism reveals that the importance ranking of convective weather
24 forecasting factors arranged by machine learning methods largely aligns with the subjective
25 understanding of forecasters. For example, the total precipitable water (PWAT) is identified as a critical
26 factor for short-term heavy precipitation forecasting, regional factors have significant impacts on
27 convective weather, and vertical motion at 300 hPa provides dynamic lifting conditions for convection.
28 This objective analysis of factor ranking not only further confirms the effectiveness of machine learning
29 in automatically extracting convective weather features but also validates the rationality of the sample
30 set construction. Overall, the use of the CNN-BiLSTM-AM model in convective weather forecasting



31 demonstrates superior performance compared to traditional machine learning algorithms and subjective
32 forecasting methods.

33 **1 Introduction**

34 The forecasting of severe convective weather primarily focuses on violent weather phenomena that occur
35 on small spatial and temporal scales, including hail, thunderstorms, strong winds, short-duration heavy
36 rainfall, tornadoes, and other hazardous and dangerous weather conditions. Due to the regional intensity
37 and rapid development characteristics of severe convective weather, forecasting is extremely challenging
38 (Han et al., 2009; Zheng et al., 2015). Such weather often has a high intensity that can potentially cause
39 severe casualties and property losses (Wang et al., 2007). For instance, the "Eastern Star" ship sinking
40 incident in 2015 (Zheng et al., 2016a), the EF4 level tornado event in Funing, Jiangsu in 2016 (Zheng et
41 al., 2016b), and the massive "720" rainstorm event in Zhengzhou, Henan in 2021 (Gao et al, 2022). In
42 monitoring and predicting severe convective weather, traditional methods that solely rely on statistical
43 results or forecaster experience exhibit significant limitations. Firstly, the occurrence condition and
44 threshold characteristics of severe convective weather will undoubtedly vary among regions with
45 different seasons, terrains, and climatic backgrounds. This diversity makes it challenging to use a unified
46 set of physical quantity thresholds to predict categories of severe convective weather in various areas.
47 Secondly, the volume of data needed to be processed during weather forecasting is considerable, and the
48 features and threshold ranges of physical quantities extracted by forecasters through statistics or
49 subjective judgement may not fully capture beneficial information or subtle changes in the data,
50 especially those at smaller scales. Additionally, due to the complex variations of severe convective
51 weather, if forecasters lack comprehensive and profound understanding of the rules governing the
52 development of severe convection, they are unable to completely grasp the useful features during the
53 development process of such weather. Even though some objective forecasting algorithms exist based
54 on physical principles and statistical properties of relevant physical quantities, thoroughly extracting
55 these features remains challenging. Moreover, when extracting features of physical quantities,
56 forecasters' abilities are constrained by their experiential knowledge and understanding.

57 The brisk advancement of artificial intelligence in recent years has spurred changes across numerous
58 domains. Notably, AI algorithms underpinned by deep learning and machine learning have achieved



59 substantial progress and found effective applications across diverse sectors. The integration of these
60 algorithms with meteorological big data often forms an efficacious toolset for severe convective weather
61 forecasting (McGovern et al., 2017; Reichstein et al., 2019). Li et al. (2018) successfully employed the
62 random forest algorithm to categorize potential severe convective weather phenomena. Based on this,
63 they developed forecasting models for short-duration intensive rainfall, thunderstorms, hail, and severe
64 convection. The training of these models involved leveraging convective indices and physical quantities
65 possessing explicit physical meanings. Furthermore, they integrated real-time forecast field data from
66 NCEP's Global Forecast System (GFS) into their predictions. The forecast outcomes of 85 severe
67 convective occurrences indicated a total misjudgment rate of 21.9% with zero omissions, thereby
68 confirming the model's extensive suitability for severe convective weather predictions. Herman et al.
69 (2018) employed NOAA's global ensemble forecast system data to construct a machine learning model
70 by using the random forest algorithm. This model encapsulates not only numerical forecasting elements
71 like convective indices, temperature, pressure, humidity, and wind field but also includes numerous
72 background forecasting components such as the maximum, minimum, median, longitude, and latitude
73 values of 1-year and 10-year average recurrence intervals (ARIs). This model has proven successful in
74 predicting extreme precipitation events 2-3 days ahead. Using the Bayesian approach, Liu et al. (2019)
75 conducted correlation analysis for thermal and dynamic factors within high-frequency lightning storm
76 cloud processes. Their findings underscored convective potential energy, convective inhibitory energy,
77 and low-level wind shear as the most influential forecasting factors – providing crucial insights for high-
78 frequency lightning storm cloud predictions. In contrast to traditional machine learning algorithms (e.g.,
79 shallow neural networks, random forest), deep learning is capable of modeling intricate nonlinear
80 systems and offering superior levels of abstraction. Importantly, deep learning can express broad function
81 sets unattainable by shallow networks more flexibly and succinctly. It demonstrates substantial
82 superiority over traditional methodologies across various fields, including speech processing and image
83 recognition (Krizhevsky et al., 2012; Lecun et al., 1995; Szegedy et al., 2013). Deep learning has also
84 found initial applications in short-term meteorological forecasting. For example, Lin et al. (2019) built a
85 Convolutional Long Short-Term Memory (ConvLSTM) model based on the Weather Research and
86 Forecasting (WRF) model and lightning data to extract spatiotemporal characteristics for future 12-hour
87 lightning predictions. Similarly, Gope (2016) constructed a rainstorm prediction model using deep neural



88 networks (specifically, stacked autoencoders) based on historical climatic data, capable of forecasting
89 intense rainfall scenarios in regions like Mumbai and Kolkata, India, 6 to 48 hours in advance.
90 With the continuous improvement of small and medium-scale observation networks, the gradual
91 enrichment of observational methods, and the rapid growth of observational data, exploring the
92 occurrence and development mechanisms in each severe convective weather process, identifying
93 characteristic parameters and threshold ranges of various types of severe convective weather from a large
94 amount of numerical model data, and comprehensively considering the geographical and climatic
95 environment of each region have become key factors for effective forecasting of severe convective
96 weather. Deep learning algorithms can automatically extract important features from big data, deeply
97 extract effective information, and comprehensively consider geographical and climatic differences across
98 regions, which will significantly optimize the results of severe convective weather forecasting. The latest
99 Pangu-Weather model is capable of predicting meteorological elements, including temperature, wind
100 speed, and pressure, with high accuracy and fast prediction speed (Bi et al., 2023). Based on the
101 reanalysis and forecast data from NCEP GFS global numerical model, our research uses deep learning
102 algorithms to establish a severe convective weather forecasting model and objective forecasting method
103 that can provide real-time objective forecast products nationwide.

104 **2 Data and methods**

105 **2.1 NCEP FNL analysis data**

106 The training and testing data in this study were obtained from the NCEP GFS 0.25°×0.25°FNL (final)
107 analysis data for the period of 2015-2020. The NCEP FNL analysis data provides global analysis fields
108 four times daily (02:00, 08:00, 14:00, and 20:00). The selection of forecast factors includes not only
109 basic meteorological elements such as temperature, geopotential height, humidity, and wind field, but
110 also commonly used physical quantities reflecting conditions related to water vapor, dynamics, and
111 energy, such as precipitable water (PWAT), Convective inhibition (CIN), and K-index (Tian et al., 2015).
112 Additionally, in order to consider geographical variations in convective activity, features such as
113 elevation, longitude, and latitude are included, resulting in a total of 144 features (see Table 1) to be
114 analyzed.

115 **Table 1. The selection of parameters**



| | parameters | level/(hPa) |
|---|---|------------------------------------|
| Multi-level physical quantities | T (Temperature) 、 TD (Dew point) | 1000、 925、 850、 700、 500、 300、 200 |
| | H (Potential height) | |
| | Wind_Speed、 Wind_Direction、 W (P-coordinate system vertical velocity) | |
| | Rh (Relative humidity) 、 TDD (Temperature dew point difference) 、 Q (Specific humidity) 、 VAPFLUXDIV (Water vapor flux divergence) | |
| | PV (Potential vorticity) 、 TMPADV (Temperature advection) 、 SITASE (Pseudo-equivalent potential temperature) 、 DIV (divergence) 、 VOR (vorticity) 、 VORADV (vorticity advection) | |
| Commonly used strong convective physical quantities | BCAPE (Bulk Convective Available Potential Energy) 、 BLI (Bulk Lifted Index) 、 CIN (Convective inhibition) 、 DCAPE (Downdraft Convective Available Potential Energy) 、 K (K-index) 、 LI (Lifted Index) 、 Z0 (Altitude of the 0 °temperature layer) 、 Z20 (Altitude of the -20 °temperature layer) 、 PWAT (Precipitable water) 、 SHIP (Large hail index) (Allen et al, 2015) 、 SHR1 (0-1km wind shear) 、 SHR3 (0-3km wind shear) 、 SHR6 (0-6km wind shear) 、 SI (Sha index) 、 TOAT (Total Index) | |
| Other quantities | ELEVATION、 LON (Longitude) 、 LAT (Latitude) | |

116 **2.2 Severe convective weather data**

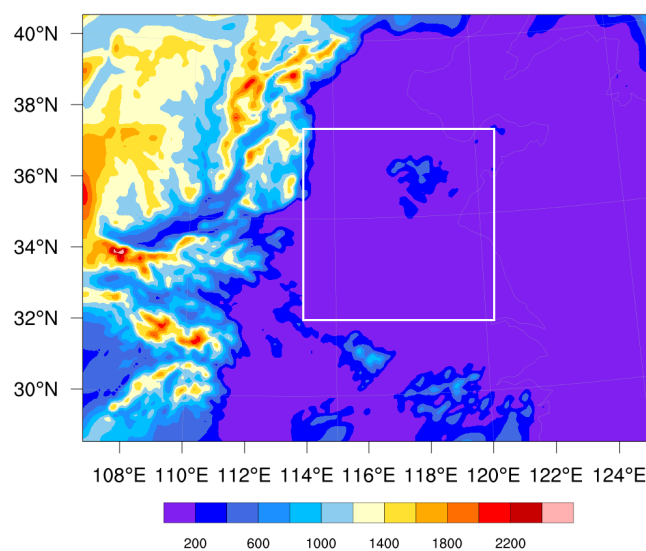
117 In this study, the convective data used were sourced from observational data collected by Chinese surface
 118 meteorological stations and archived by the National Meteorological Information Center. The National
 119 Meteorological Information Center performs quality checks and error data corrections on timed
 120 observations and daily extreme value data for 19 major elements, including temperature, pressure,
 121 precipitation, humidity, and sunshine duration, from over 2400 ground stations nationwide. This process



122 addresses systematic issues that may arise during the digitization process, such as data omissions or
123 duplication. The data undergoes three levels of quality control review at the station, provincial, and
124 national levels within the routine operations of the meteorological data departments.

125 2.3 Selection of experimental area

126 The Henan region is not only one of China's important agricultural production areas but also a zone
127 where modern cities and rural areas coexist with complex terrain due to extensive industrial development.
128 Furthermore, being located in the mid-latitudes, Henan frequently experiences cold air invasions, while
129 warm and humid air masses can also reach the region during the summer, often leading to intense rainfall
130 events resulting from the convergence of warm and cold air masses. Additionally, numerous signs
131 indicate that China's climate is entering a transitional period, potentially leading to a shift from low
132 rainfall in summer to higher rainfall in northern regions. Therefore, selecting the Henan region (as
133 illustrated in Figure 1) as the study area for this research is highly appropriate. Undoubtedly, it will lay
134 the foundation for future improvements in severe weather warnings and disaster prevention and
135 mitigation capabilities in the region, reflecting a forward-looking study with a strategic perspective.



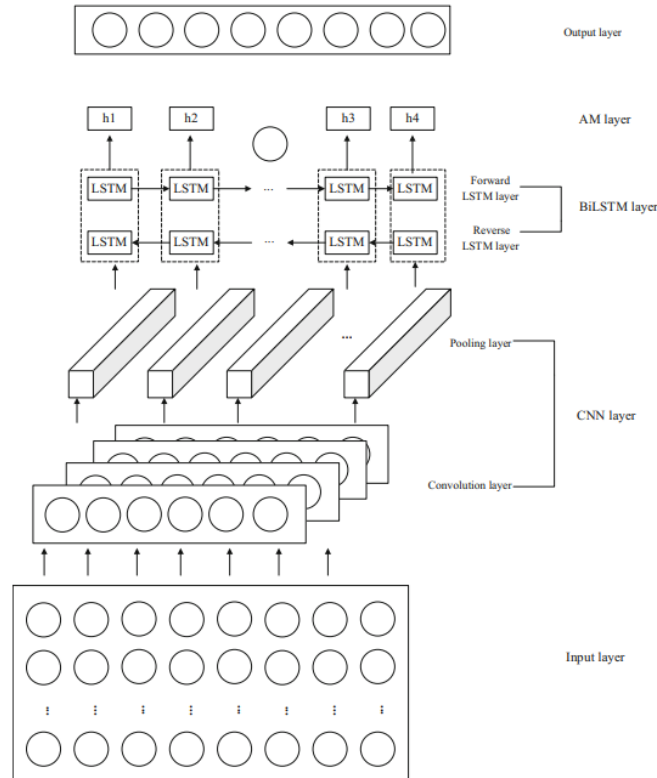
136
137 **Figure 1: The selected area of experiment (The white rectangle denotes the selected area: Henan, 31° -37°**
138 **N, 110° -117° E); Distribution of topography (shaded; unit: m)**



139 **3 Deep learning model**

140 **3.1 Deep learning model structure**

141 To forecast severe convective weather more accurately, this study develops a CNN-BiLSTM-AM-based
142 model for convective prediction. The model consists of Convolutional Neural Network (CNN),
143 Bidirectional Long Short-Term Memory (BiLSTM), and Attention Mechanism (AM). The CNN extracts
144 features from the input inventory data, while the BiLSTM effectively captures the interdependencies in
145 the temporal sequence data. The AM is a mechanism that improves results by capturing the impact of
146 past feature states on heavy rainfall. The model primarily comprises the CNN, BiLSTM, and AM layers,
147 including an input layer, CNN layer (with one-dimensional convolutional and pooling layers), BiLSTM
148 layer (with forward and backward LSTM layers), AM layer, and output layer (see Figure 2 for details)(Lu
149 et al, 2021). During weather forecasting, we analyze historical meteorological images and numerical
150 products to draw conclusions. To summarize this process briefly, we first analyze meteorological images
151 or various forecast products to generate situational forecasts. Then, combining the situational forecasts
152 with local real-time meteorological data, we obtain element forecasts. If we simplify these two steps
153 further, the first step involves extracting features from meteorological images or forecast products (i.e.,
154 situational forecasting), and the second step involves fitting the extracted features with local historical
155 meteorological information to obtain the required forecast values (i.e., element forecasting). In the CNN-
156 BiLSTM-AM model, these two steps are transformed accordingly: using the CNN for data feature
157 extraction and subsequently applying the BiLSTM and AM to match historical meteorological
158 information in order to derive the element values. Prior to inputting the data into the CNN-BiLSTM-AM
159 model, we normalize the data and convert it into matrix form. Once these settings are completed, the
160 model can be trained.



161

162 **Figure 2: CNN-BiLSTM-AM model structure diagram**

163 The training process of CNN-BiLSTM-AM is illustrated in Figure 3, with the main steps outlined as
 164 follows:

- 165 1) Input Data: Provide the necessary data for training CNN-BiLSTM-AM.
 166 2) Input Data Normalization: To enhance model training performance, the input data is standardized due
 167 to its significant variations. The normalization formula is expressed as Equation (1):

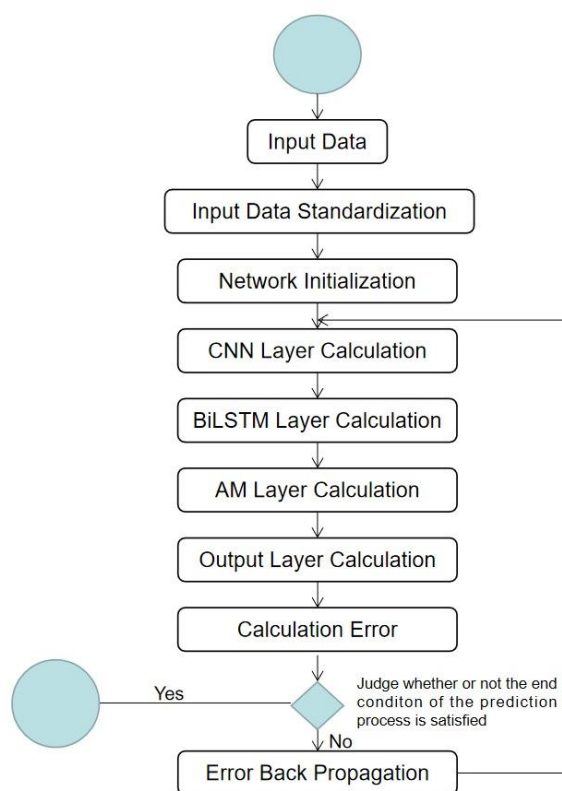
$$y_i = \frac{x_i - \bar{x}}{s} \quad (1.1)$$

168 Among them, y_i is the standardized value, x_i is the input data, \bar{x} is the average value of the input data,
 169 and s is the standard deviation of the input data.

- 170 3) Network Initialization: Initialize the weights and biases of each layer in CNN-BiLSTM-AM.
 171 4) CNN Layer Computation: Pass the input data sequentially through the convolutional and pooling
 172 layers within the CNN layer to extract features and obtain output values.



- 173 5) BiLSTM Layer Computation: Use the hidden layer of the BiLSTM layer to compute the output data
174 from the CNN layer and obtain output values.
- 175 6) AM Layer Computation: Compute the output data from the BiLSTM layer using the AM layer and
176 obtain output values.
- 177 7) Output Layer Computation: Calculate the output value of the model by computing the output value
178 of the AM layer.
- 179 8) Error Calculation: Compare the computed output value from the output layer with the true value of
180 the data set and calculate the corresponding error.
- 181 9) Check if the termination conditions for the training process are met: Successful termination conditions
182 include completing a predetermined number of cycles, reaching a weight below a certain threshold, or
183 achieving a prediction error rate below a specific threshold. If any of these conditions are met, the training
184 is completed; otherwise, the training continues.
- 185 10) Error Backpropagation: Propagate the calculated error in the opposite direction, updating the weights
186 and biases of each layer, and then return to step 4 to continue the training.



187
188 **Figure 3: Flow chart of CNN-BiLSTM-AM training process**

189 The prediction process of CNN-BiLSTM-AM is illustrated in Figure 4 and consists of the following
190 main steps:

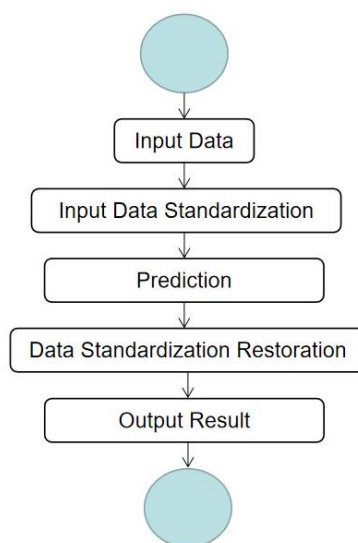
- 191 1) Input Data: Provide the input data required for prediction.
- 192 2) Data Standardization: Normalize the input data.
- 193 3) Prediction: Feed the standardized data into the trained CNN-BiLSTM-AM model and obtain the
194 corresponding output values.
- 195 4) Data Standardization Recovery: The output values obtained from CNN-BiLSTM-AM are in
196 standardized form. To restore them to their original values, apply Equation (2) to convert the standardized
197 values back.

$$x_i = y_i * s + \bar{x} \quad (1.2)$$



198 Among them, x_i represents the recovered value of the standardized value, y_i represents the output
199 value of CNN-BiLSTM-AM, s represents the standard deviation of the input data, and \bar{x} represents the
200 mean value of the input data.

201 5) Output Results: Present the recovered results after restoration as the completion of the prediction
202 process.



203
204 **Figure 4: Flow chart of CNN-BiLSTM-AM prediction process**

205 3.2 Construction of training and testing datasets

206 The prediction of severe convective weather can be viewed as a binary classification problem,
207 distinguishing between its occurrence (labeled as 1) and non-occurrence (labeled as 0). Consequently,
208 we can utilize actual severe weather data to calibrate the numerical analysis field, thus constructing
209 training and testing sample datasets. Since NCEP FNL provides both analyzed and forecasted grid-based
210 fields while the observed data is in scattered form, the observed data needs to be gridded. If a related
211 weather event occurs within a grid radius of R , it is considered that the event occurs at that grid point
212 (labeled as 1); otherwise, it is considered that the event does not occur at that grid point (labeled as 0).
213 Considering that convective weather is typically associated with mesoscale weather systems, we
214 conducted experiments and determined to use $R=20\text{km}$. Setting R too small may result in missing severe
215 convective events, whereas setting it too large may lead to false alarms.



216 The occurrence probability of severe convective weather is relatively low, resulting in a significant class
217 imbalance where positive samples (i.e., samples with severe convective events) are much fewer than
218 negative samples (i.e., samples without severe convective events). This presents a typical issue of
219 imbalanced data (Krawczyk et al., 2016). To address this, we employed the oversampling technique
220 (Buda et al., 2017) by randomly duplicating positive samples to achieve a balanced distribution between
221 positive and negative samples. With this approach, we constructed the training and testing datasets using
222 real-time data from January to December between 2015 and 2020, as well as NCEP FNL data. The testing
223 dataset consisted of one randomly selected day from each month during the aforementioned period,
224 totaling 72 days, while the training dataset comprised the remaining samples. During the training process,
225 we utilized the ADAM optimizer (Kingma and Ba, 2014) with a learning rate set at 10^{-4} , and default
226 values were used for other settings (Perol et al., 2017). The CNN-BiLSTM-AM model was trained for
227 30 epochs with a batch size of 64. Through training and parameter tuning, we obtained the optimal
228 prediction model. This model can incorporate NCEP FNL data and transform features into a four-
229 dimensional array of $M \times 28 \times 32 \times 1$ (M represents the number of samples), enabling predictions for severe
230 convective weather.

231 4 Results

232 4.1 Evaluation methods

233 Commonly used verification measures for evaluating forecast results include the Probability of Detection
234 (POD), the Threat Score (TS), the Equitable Threat Score (ETS), the Bias (BIAS), the False Alarm Ratio
235 (FAR), and the Missed Alarm Ratio (MAR). These measures are defined as follows:

$$\text{POD} = \frac{h}{h + m} \quad (1.3)$$

$$\text{TS} = \frac{h}{h + m + f} \quad (1.4)$$

$$\text{ETS} = \frac{h - h_{\text{random}}}{h + f + m + -h_{\text{random}}}, h_{\text{random}} = (h + f) * (h + m) / (h + m + f + c) \quad (1.5)$$

$$\text{BIAS} = \frac{h + f}{h + m} \quad (1.6)$$



$$\text{FAR} = \frac{f}{h + f} \quad (1.7)$$

$$\text{MAR} = \frac{m}{h + m} \quad (1.8)$$

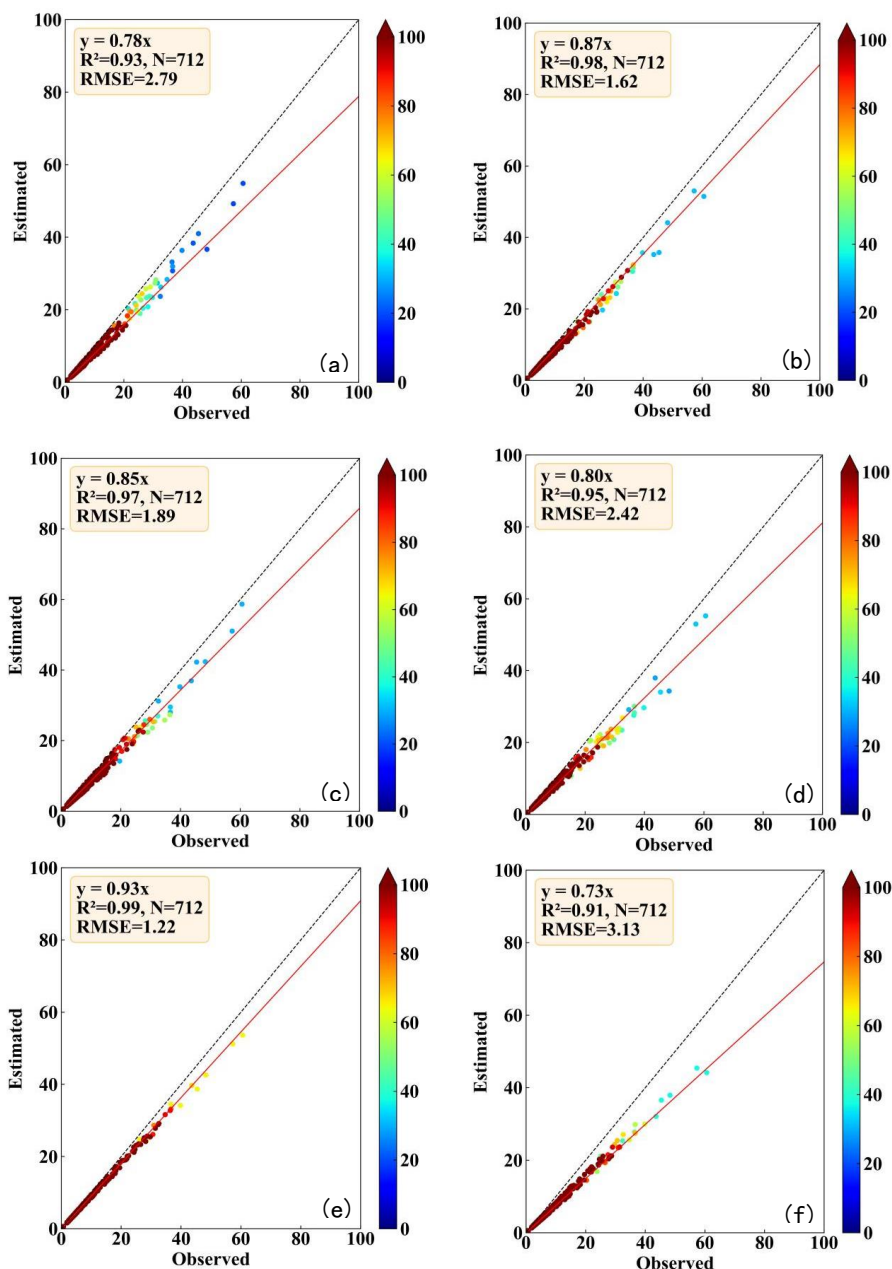
236 Among them, h represents the number of occurrences when both the forecast and observed events appear,
237 m represents the number of occurrences when the observed event appears but the forecast does not, f
238 represents the number of occurrences when the forecast event appears but the observed event does not,
239 and c represents the number of occurrences when neither the forecast nor the observed event appears.

240 **4.2 Evaluation of different models**

241 To investigate the differences between the CNN-BiLSTM-AM model and traditional machine learning
242 algorithms, this study compared their forecasting performance on convective weather test dataset from
243 2015 to 2017. Figure 5 presents a comparative analysis of predicted and observed precipitation between
244 the observations and various models. The figure suggested that the SVM and KNN methods resulted in
245 subpar precipitation prediction, as evidenced by their relatively high RMSE values of 2.42mm and
246 2.79mm respectively. Compared to the WRF model, these figures represent reductions of 22.68% and
247 10.86%. Additionally, the correlation coefficients between the predicted and actual precipitation were
248 low due to more dispersed distributions. On the contrary, RF and GBDT methods demonstrated superior
249 performance in precipitation prediction. They achieved smaller RMSE values between the predicted and
250 actual rainfall, reaching 1.62mm and 1.89mm respectively, representing reductions of 48.24% and 39.62%
251 when compared with the WRF model. These methods also exhibited stronger correlations, indicated by
252 higher correlation coefficients, suggesting concentrated distributions of predicted rainfall and actual
253 precipitation errors. However, despite the promising results obtained by RF and GBDT methods, the
254 CNN-BiLSTM-AM model proposed in this study outperformed them. The distribution of the predicted
255 and actual precipitation using the CNN-BiLSTM-AM method was notably more concentrated, leading
256 to the smallest overall error. Specifically, the RMSE value for the CNN-BiLSTM-AM model was merely
257 1.22mm, marking reductions of 61.02%, 49.59%, 56.27%, 35.45%, and 24.9% in comparison to WRF,
258 SVM, KNN, GBDT, and RF models respectively. Furthermore, it reached an impressive correlation
259 coefficient of approximately 99% between the predicted precipitation and the actual data. Based on this
260 evidence, it is clear that the CNN-BiLSTM-AM model substantially surpasses traditional machine-



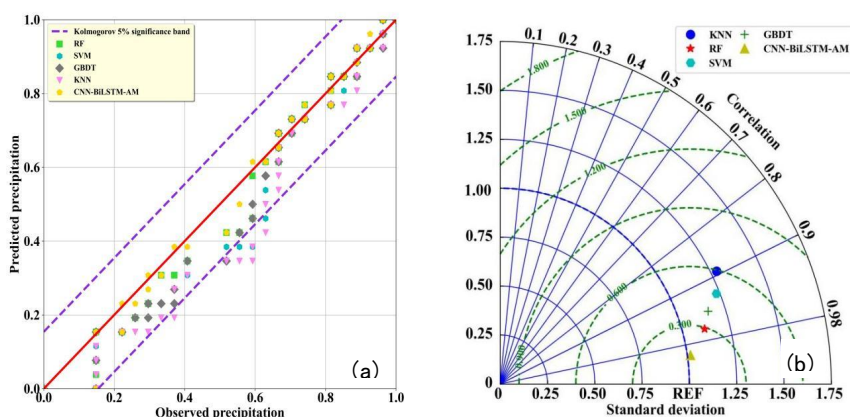
261 learning algorithms such as SVM, KNN, GBDT, and RF in the context of precipitation prediction.



262
263 **Figure 5: Scattered density plots of the observed and machine-learning corrected precipitation (a: 10-fold**
264 **cross-validation training dataset of KNN model, b: 10-fold cross-validation training dataset of RF model, c:**
265 **10-fold cross-validation training dataset of GBDT model, d: 10-fold cross-validation training dataset of SVM**
266 **model, e: CNN-BiLSTM-AM model forecasts, and f: WRF forecasts)**



267 To further investigate the reliability of the CNN-BiLSTM-AM model, we compared it with the other five
268 models using the cumulative distribution probability scatter plots and Taylor plots, and the results were
269 shown in Figure 6. From the data provided in the figure, it was evident that the CNN-BiLSTM-AM
270 model outperforms the other models significantly. It exhibited a standard deviation of 1.02 and a
271 correlation coefficient of 0.99. Following closely behind as the second most accurate model is the RF
272 model, boasting a standard deviation of 1.12 and a correlation coefficient of 0.97. The KNN model
273 demonstrated the weakest performance, with a standard deviation and correlation coefficient of 1.26 and
274 0.90 respectively. The accuracy metrics of the SVM, and GBDT models fell between those of the
275 superior (CNN-BiLSTM-AM and RF) and inferior (KNN) models. Specifically, their standard deviations
276 and correlation coefficients were recorded as follows: SVM - 1.24 and 0.91; GBDT - 1.20 and 0.94. In
277 conclusion, the CNN-BiLSTM-AM model held a distinct advantage in its ability to effectively extract
278 the development characteristics of convective weather, thereby achieving superior precipitation
279 prediction.



280
281 **Figure 6: The cumulative distribution probability scatter plots of the observed precipitation and the predicted**
282 **precipitation of 6 models(a) ; Taylor distribution plot of different model performance(b)**

283 4.3 Individual Case Forecast Evaluation

284 On July 22, 2022, widespread thunderstorms and short-term heavy precipitation occurred in Henan and
285 central Inner Mongolia, China. The forecast performance of this weather process is illustrated in Table
286 2 and Figure 7. From the comparison of various prediction methods in the table, we can conclude that:
287 Regardless of whether it was the CNN-BiLSTM-AM model or other algorithms such as Gradient



288 Boosting Decision Trees (GBDT), Random Forests (RF), Support Vector Machines (SVM), or K-Nearest
289 Neighbors (KNN), the forecast performance for convective weather showed a decreasing trend with
290 increasing forecast duration. Additionally, the Probability of Detection (POD) and Threat Score (TS)
291 significantly decreased, while the False Alarm Ratio (FAR) significantly increased. This can be attributed
292 to the nonlinear and complex nature of convective system development, which leads to diminishing
293 predictability with longer forecast durations. Among the five learning models tested, the CNN-BiLSTM-
294 AM model demonstrated the best predictive performance in the 2-6 hour forecast duration. For example,
295 within the 2-6 hour time range, the POD, Equitable Threat Score (ETS), and TS values for the CNN-
296 BiLSTM-AM model were 0.550, 0.524, 0.484, 0.470, 0.463, 0.495, 0.453, 0.384, 0.310, 0.245, and 0.440,
297 0.375, 0.338, 0.306, 0.226, respectively. Compared to the second-ranked RF model, they improved by
298 15.30%, 23.88%, 17.48%, 16.34%, 19.64%, 21.32%, 26.89%, 21.52%, 14.81%, 20.69%, and 17.33%,
299 23.76%, 25.19%, 60.21%, 88.33%. Overall, the CNN-BiLSTM-AM model showed a significant
300 improvement in forecast performance compared to other machine learning algorithms. As the forecast
301 duration increased, the CNN-BiLSTM-AM model outperformed other machine learning models in terms
302 of forecast results. For example, at the 3rd hour, the difference in TS values between the CNN-BiLSTM-
303 AM model and GBDT, RF, SVM, KNN models were 0.129, 0.072, 0.152, 0.163, representing
304 improvements of 52.44%, 23.76%, 68.16%, 76.89%. At the 6th hour, the corresponding TS differences
305 were 0.110, 0.106, 0.111, 0.112, showing improvements of 94.83%, 88.33%, 96.52%, 98.25%. Therefore,
306 it can be observed that beyond the 2-hour forecast stage, the CNN-BiLSTM-AM model performs more
307 prominently in convective weather forecasting. The figure 6 clearly illustrates the variations in forecast
308 performance across different models. In the 1-hour forecast duration, both deep learning and machine
309 learning algorithms did not exhibit significant changes in forecast performance. This can be attributed to
310 the fact that within the 0-1 hour time range, convective system morphology undergoes minimal changes,
311 and the NCEP fnl analysis data contains sufficient information about the initial stage of convection,
312 allowing effective prediction relying solely on analysis data. However, within the 2-6 hour forecast
313 duration, the CNN-BiLSTM-AM model consistently outperformed the machine learning methods,
314 particularly as the lead time extended. The performance gap between the CNN-BiLSTM-AM model and
315 other machine learning models gradually widened. This indicates that the CNN-BiLSTM-AM model
316 possesses nonlinear evolution recognition and prediction capabilities, with its provided information



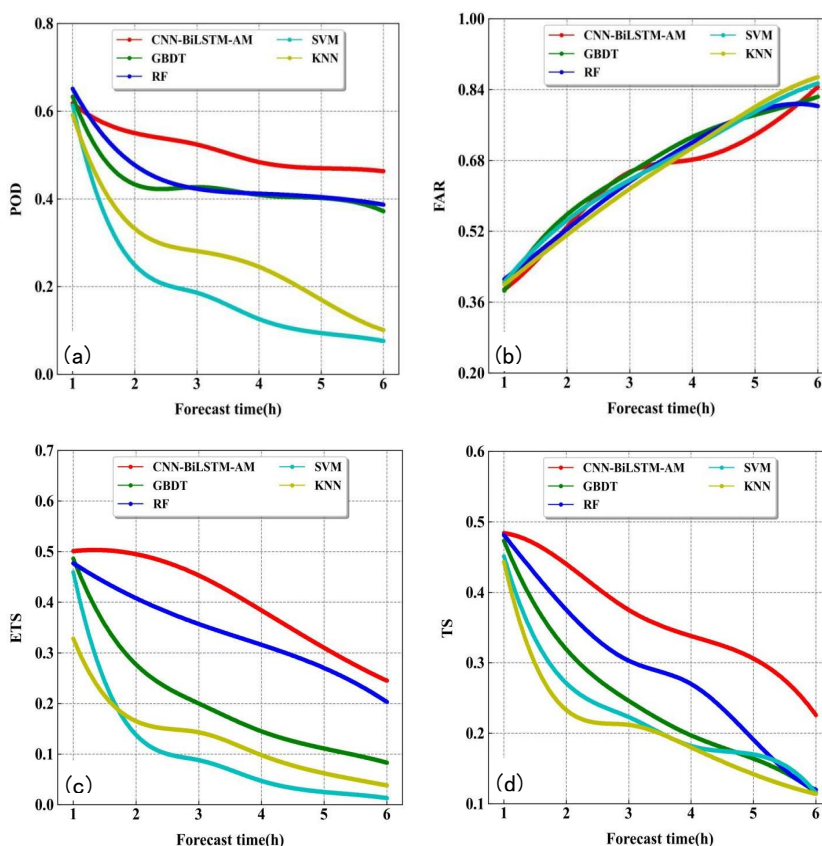
317 becoming more valuable as the forecast duration increases. These findings further confirm the
 318 advantages of deep learning methods in severe convection forecasting.

319 **Table 2. Comparison of various models on convective weather case on July 22, 2022**

| Models | Forecast duration | POD | FAR | ETS | TS |
|---------------|-------------------|-------|-------|-------|-------|
| CNN-BiLSTM-AM | 1h | 0.618 | 0.389 | 0.501 | 0.484 |
| | 2h | 0.550 | 0.430 | 0.495 | 0.440 |
| | 3h | 0.524 | 0.454 | 0.453 | 0.375 |
| | 4h | 0.484 | 0.482 | 0.384 | 0.338 |
| | 5h | 0.470 | 0.538 | 0.310 | 0.306 |
| | 6h | 0.463 | 0.646 | 0.245 | 0.226 |
| GBDT | 1h | 0.633 | 0.386 | 0.486 | 0.473 |
| | 2h | 0.433 | 0.558 | 0.277 | 0.319 |
| | 3h | 0.427 | 0.652 | 0.200 | 0.246 |
| | 4h | 0.409 | 0.733 | 0.145 | 0.197 |
| | 5h | 0.402 | 0.783 | 0.111 | 0.164 |
| | 6h | 0.372 | 0.824 | 0.083 | 0.116 |
| RF | 1h | 0.651 | 0.412 | 0.477 | 0.481 |
| | 2h | 0.477 | 0.525 | 0.408 | 0.375 |
| | 3h | 0.423 | 0.632 | 0.357 | 0.303 |
| | 4h | 0.412 | 0.721 | 0.316 | 0.270 |
| | 5h | 0.404 | 0.790 | 0.270 | 0.191 |
| | 6h | 0.387 | 0.803 | 0.203 | 0.120 |
| SVM | 1h | 0.413 | 0.405 | 0.459 | 0.451 |
| | 2h | 0.249 | 0.545 | 0.138 | 0.271 |
| | 3h | 0.186 | 0.636 | 0.088 | 0.223 |
| | 4h | 0.126 | 0.710 | 0.047 | 0.182 |
| | 5h | 0.094 | 0.790 | 0.025 | 0.170 |
| | 6h | 0.076 | 0.854 | 0.013 | 0.115 |
| KNN | 1h | 0.391 | 0.400 | 0.328 | 0.253 |



| | | | | |
|----|-------|-------|-------|-------|
| 2h | 0.332 | 0.512 | 0.165 | 0.443 |
| 3h | 0.281 | 0.616 | 0.143 | 0.212 |
| 4h | 0.245 | 0.709 | 0.098 | 0.180 |
| 5h | 0.170 | 0.801 | 0.062 | 0.142 |
| 6h | 0.101 | 0.868 | 0.038 | 0.114 |



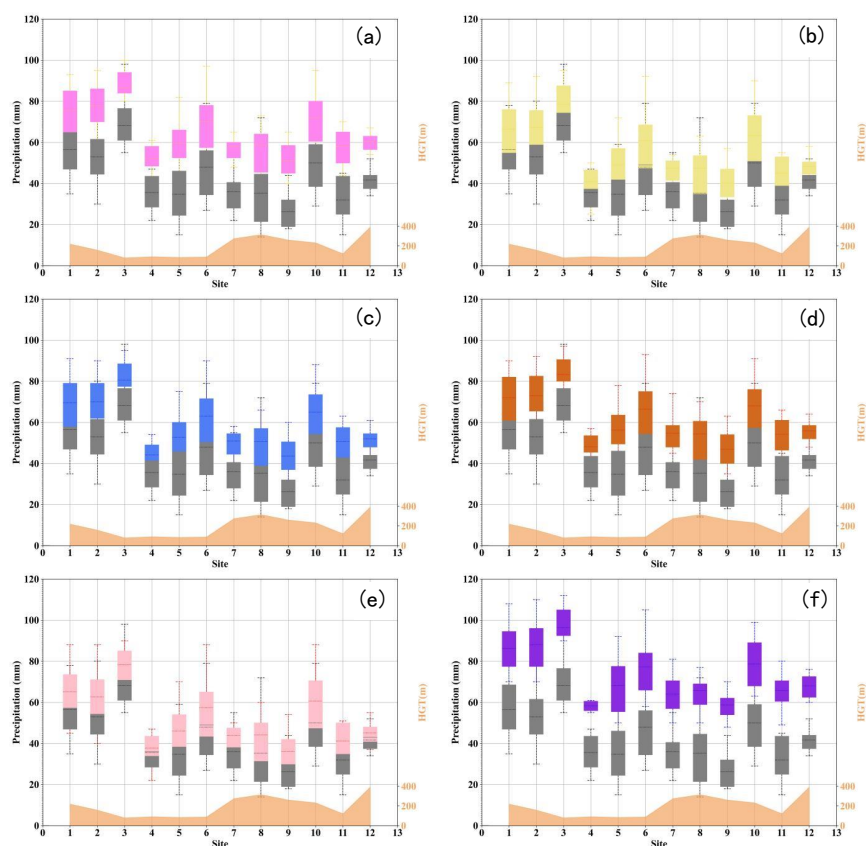
320

321 **Figure 7: Comparison of forecast performance of different models**

322 To assess how errors vary in different models, we selected Zhengzhou in Henan as specific region for
 323 evaluation and analysis. The boxplots of the predicted precipitation and the actual precipitation of 6
 324 models at 12 stations in Zhengzhou show that (see Figure 8), the CNN-BiLSTM-AM gave more accurate
 325 results than the other models, its difference between the observed precipitation and the predicted
 326 precipitation was very small, which is significantly superior to those of the other models; For the RF and
 327 GBDT models, the difference between the observed precipitation and the predicted precipitation was not



328 significant and both showed better performance than KNN and SVM models. Overall, the CNN-
329 BiLSTM-AM model showed the best performance with higher accuracy for all stations, and the KNN
330 and SVM model illustrated the lowest performance among other models and approaches.



331
332 **Figure 8: The boxplots of the predicted precipitation of the KNN(a), RF(b), GBDT(c), SVM(d), CNN-**
333 **BiLSTM-AM(e), and WRF(f) models at 12stations and the boxplots of the actual precipitation (gray).**

334 4.4 Spatial-temporal variations in the best model

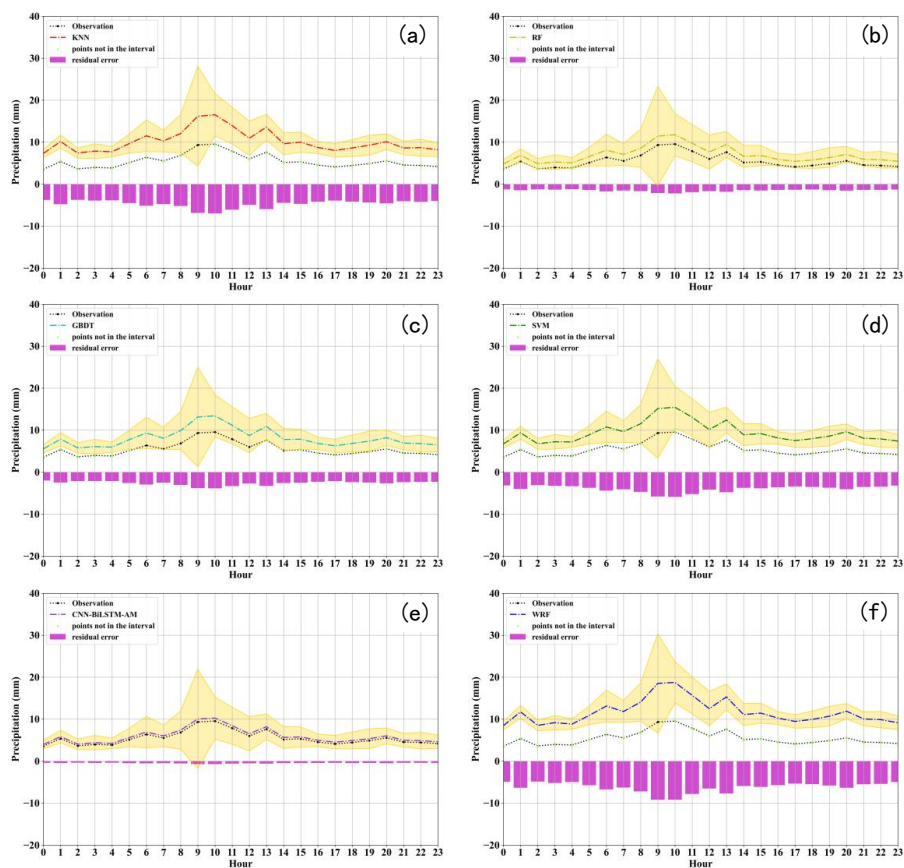
335 Figure 9 depicts the diurnal variations offered by diverse models in July 2022, and also shows the diurnal
336 fluctuation in precipitation in the initial WRF forecast. The precipitation forecast by the original WRF
337 weather prediction model exhibits noticeable inaccuracies. As can be seen from the figure, WRF's
338 precipitation forecast displays a distinct diurnal variation trait, characterized by substantial discrepancies
339 between early morning and afternoon hours, namely between 9:00 am and 13:00 pm (Figure 9f). This



340 indicates that WRF's precipitation forecast tends to be inaccurate and displays significant errors in diurnal
341 variation.

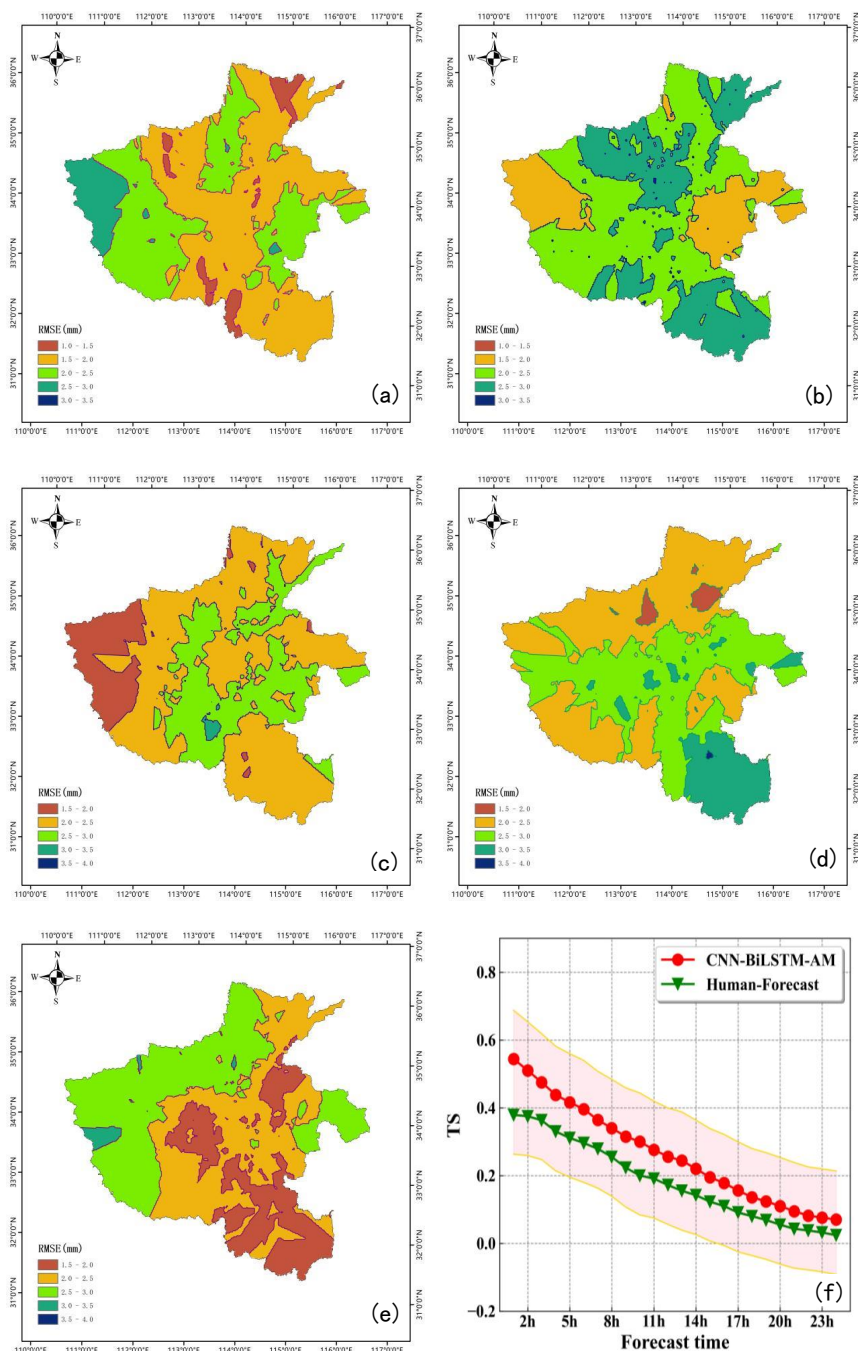
342 Compared to the precipitation forecast results of different ML models, the diurnal variation error was
343 considerably lessened (Figure 9a, b, c, d, and e). Initially, the mean precipitation forecast by the CNN-
344 BiLSTM-AM model aligns well with the actual average precipitation trajectory, with minimal error and
345 devoid of diurnal variation (Figure 9e). This suggests that the predicted and actual distributions of
346 precipitation are in agreement. However, the results performed between 9:00 am and 13:00 pm during
347 January 2021 were not very satisfactory. This could be attributed to the inadequate generalization
348 abilities of the training model and the excessive volatility of actual precipitation at these specific times.
349 Based on the above comparative analysis, it can be inferred that the CNN-BiLSTM-AM model
350 outperforms other models.

351 In order to facilitate a more intuitive comparison, we visualized the distribution of forecast results for
352 different models (see Figure 10). As can be seen from Figure 10, the RMSE (Figure 10a, b, c, d, and e)
353 distribution of precipitation of 5 models show that the performance of the CNN-BiLSTM-AM model is
354 better than the other machine learning models, RMSE value is mostly between 0.11mm and 3.87mm.
355 The performances of the RF, SVM, GBDT, and KNN models are not as good as CNN-BiLSTM-AM,
356 their RMSE were recorded as follows: RF: 0.10mm-4.25mm, SVM: 0.38mm-4.31mm; GBDT: 0.33mm-
357 4.68mm, KNN: 0.56mm-4.82mm. From the 24-hour forecast scores (Fig.8f), the CNN-BiLSTM-AM
358 model consistently outperformed the subjective predictions of the forecasters. This indicates that the
359 CNN-BiLSTM-AM model, based on deep learning techniques, significantly improved the forecast
360 accuracy for this severe convective weather event, providing forecasters with valuable guidance and
361 reference.



362
363 **Figure 9: KNN(a), RF(b), GBDT(c), SVM(d), CNN-BiLSTM-AM(e), and WRF(f) daily variation of predicted**
364 **and actual precipitation on July 2022.**

365



366
 367 **Figure 10: RMSE distribution of CNN-BiLSTM-AM(a), RF(b), SVM(c), KNN(d), GBDT(e) models in Henan;**
 368 **TS scores of strong convective weather on July 22, 2022 (f)**



369 **5 Discussion**

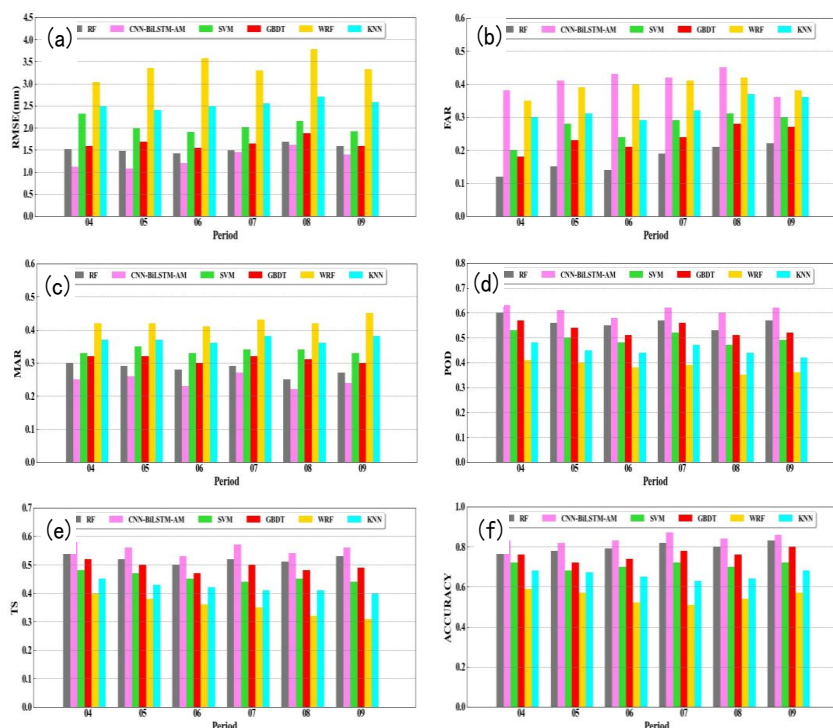
370 **5.1 Stability analysis of the proposed models**

371 The preceding results presented the visualized outcomes of various correction methods, which may not
372 fully prove the stability of different approaches. To further evaluate the stability of various machine-
373 learning models, we compared their performance on strong convective weather forecasting during the
374 flood season (April-September) from 2020 to 2022 by using six evaluation metrics: RMSE, FAR, MAR,
375 POD, TS, and accuracy. The specific results are presented in Figure 11. This comprehensive analysis
376 will provide a more accurate assessment of the stability of different models.

377 The RMSE values of the five machine-learning models were lower than that of the WRF model, with the
378 CNN-BiLSTM-AM model having the smallest RMSE of 1.12mm. This represented a 63.04% reduction
379 in RMSE compared to the output precipitation of the WRF model. From the perspective of solving
380 regression problems, the model effectively corrected the deviation in precipitation predicted by the
381 numerical forecast model. In comparison to other machine-learning algorithms, the accuracy of the CNN-
382 BiLSTM-AM model showed a significant improvement, demonstrating the stability of deep-learning
383 methods for nonlinear problems such as precipitation, often achieving superior application results.

384 FAR and MAR are two important indicators for evaluating precipitation forecasting accuracy, reflecting
385 false and missing alarm rates, respectively. As shown in the figure, the FAR of the CNN-BiLSTM-AM
386 model was higher than that of all the other corrected models, while its MAR was lower than that of all
387 the other models. This situation might be due to the fact that while the CNN-BiLSTM-AM model
388 effectively fits precipitation, it also has side effects, leading to precipitation forecasts in the absence of
389 actual precipitation. The FAR and MAR values obtained by the other four machine-learning algorithms
390 were lower than those of the WRF model, indicating that these machine-learning methods can reduce the
391 false and missing rates of the WRF model precipitation forecasts to a certain extent.

392 Finally, the POD, TS and accuracy scores of the five machine-learning models were significantly higher
393 than that of the WRF model, with the CNN-BiLSTM-AM model achieving the best performance among
394 all models. These results indicate that the CNN-BiLSTM-AM model exhibits an ideal performance in
395 correcting precipitation forecasts from the WRF model, outperforming other machine-learning methods
396 in terms of precipitation correction.



397
 398 **Figure 11: Evaluation histograms of precipitation predicted by 6 models and actual precipitation in different**
 399 **months ((a), (b), (c), (d), (e), and (f) represent RMSE(mm), FAR, MAR, POD, TS, and ACCURACY**
 400 **respectively).**

401 **5.2 Explainability of the mechanism of severe convective weather based on machine learning**

402 Although machine learning and deep learning methods have made significant breakthroughs in various
 403 fields, effectively predicting severe convective weather using these methods still remains a "black box"
 404 challenge (McGovern et al., 2019), with the specific details being difficult to ascertain. Currently, many
 405 researchers are attempting to uncover this "black box" and have developed several model interpretation
 406 and visualization (MIV) techniques. Through MIV, users of machine learning can gain a better
 407 understanding of the strengths, weaknesses, and optimal application scenarios of the models, thereby
 408 increasing trust in the models and enhancing their practicality. If the machine learning forecasts
 409 outperform human forecasters, MIV can also help improve subjective judgment and prediction results,
 410 as well as validate new scientific hypotheses and conjectures (McGovern et al., 2019). In this section,
 411 we apply a method of ranking the importance of forecast factors to analyze the forecasting process of the



412 deep learning model, aiming to unravel the mystery of the "black box" in deep learning for predicting
413 severe convective weather.

414 5.2.1 Technical method

415 By employing the Random Forest (RF) algorithm, we can conduct an importance analysis of forecast
416 factors to ascertain the significance of each predictor and establish a priority ranking. The fundamental
417 principle involves measuring the contribution of each feature in every tree within the random forest,
418 averaging these values, and then comparing the contributions among the features. Typically, we can
419 utilize the Gini index or Out-of-Bag (OOB) error rate as evaluation metrics. In this study, we solely focus
420 on the approach that employs the Gini index for assessment. Here, we denote Variable Importance
421 Measures (VIM) as the score reflecting the importance of variables, GI represents the Gini index,
422 $VIM_j^{(Gini)}$ denotes the Gini index score for the j -th feature (X_j). Assuming there are J features, $X_1, X_2,$
423 X_3, \dots, X_J , I decision trees, and C categories, the Gini index of node q in the i -th tree is calculated as
424 follows:

$$G_i^q = \sum_{c=1}^{|C|} \sum_{c' \neq c} P_{qc}^{(i)} P_{qc'}^{(i)} = 1 - \sum_{c=1}^{|C|} (P_{qc}^{(i)})^2 \quad (1.9)$$

425 Among them, C represents the categories, and P_{qc} denotes the proportion of category c at node q . The
426 change in Gini index for a feature is given by:

$$VIM_j^{(Gini)(i)} = \sum_{q \in Q} VIM_{jq}^{(Gini)(i)} \quad (1.10)$$

427 Suppose there are I trees in the Random Forest (RF), then:

$$VIM_j^{(Gini)} = \sum_{i=1}^I VIM_j^{(Gini)(i)} \quad (1.11)$$

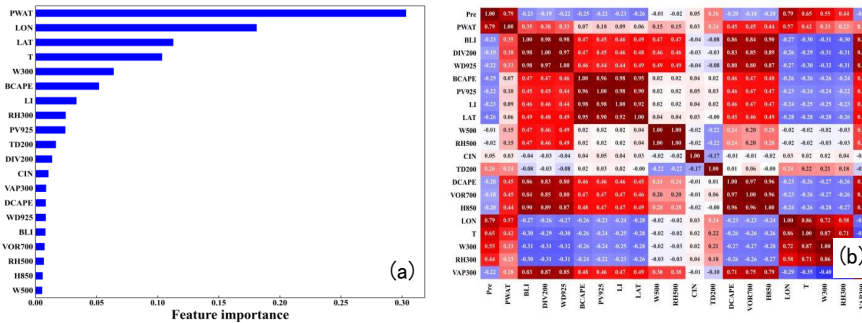
428 Finally, normalization is performed:



$$VIM_j^{(Gini)} = \frac{VIM_j^{(Gini)}}{\sum_{j'=1}^J VIM_{j'}^{(Gini)}} \quad (1.12)$$

429 5.2.2 The interpretability of machine learning models

430 Using the RF algorithm, we conducted an importance analysis of forecast factors on the training and
431 testing datasets of CNN-BiLSTM-AM model constructed by us, obtaining the relative rankings of each
432 forecast factor's importance and their corresponding correlation coefficients (see Figures 12). From the
433 figures, it is evident that moisture conditions are crucial for severe convective weather, with the most
434 important feature being precipitable water (PWAT), which significantly outweighs the second-ranked
435 feature. Geographic location also has a significant impact on severe convective weather, with longitude
436 (LON) and latitude (LAT) ranking second and third among all indicators, respectively. As convective
437 weather fundamentally arises from temperature variations, when the near-surface air absorbs sufficient
438 heat and expands, its density decreases, leading to an unstable atmosphere that triggers convective
439 weather. Therefore, the temperature (T) feature ranks fourth. Strong convection imposes certain
440 requirements on atmospheric dynamic lifting conditions, with 300hPa vertical motion (W300) ranking
441 fifth. Atmospheric energy conditions have some influence on severe convective weather but are not the
442 most important factors, as Bulk Convective Available Potential Energy (BCAPE) and Lifted Index (LI)
443 rank sixth and seventh, respectively. These features align closely with the importance distribution of
444 physical quantities related to short-term severe convective weather obtained by Tian et al. (2015) through
445 statistical analysis. Additionally, these features are consistent with the characteristics of various types of
446 severe convective weather analyzed by forecasters in terms of moisture, energy, dynamics, and other
447 conditions (Zeng & Yang, 2020; Zhang et al., 2020; Zhang et al., 2022). These results demonstrate the
448 high effectiveness of machine learning in automatically extracting features and further confirm the
449 rationality of constructing the sample dataset.



450
 451 **Figure 12: Relative importance of forecast factors (top 20 most important forecast factors); The correlation**
 452 **coefficient between each of the forecast factors**

453 **6 Summary**

454 This study utilizes the NCEP Global Forecast System (GFS) reanalysis data and forecast data to construct
 455 a CNN-BiLSTM-AM model for predicting severe convective weather using deep learning techniques
 456 and comprehensively evaluate the performance of this model. Furthermore, to gain a better understanding
 457 of the "black box" principles of deep learning for severe convective weather prediction, we visualize the
 458 training process by ranking the importance of forecast factors. The main conclusions are as follows:

459 1) Compared to traditional machine learning algorithms such as Gradient Boosting Decision Trees
 460 (GBDT), Random Forest (RF), Support Vector Machines (SVM), and K-Nearest Neighbors (KNN), the
 461 CNN-BiLSTM-AM model can automatically identify and learn deeper nonlinear features of severe
 462 convective weather. Consequently, it achieves higher prediction accuracy on the severe convective
 463 weather dataset. Moreover, as the lead time increases, all algorithms exhibit a decreasing trend in their
 464 forecasting performance.

465 2) In comparison to subjective forecasts made by meteorologists, the CNN-BiLSTM-AM model
 466 demonstrates good performance in forecasting severe convective weather, with improvements in scoring
 467 metrics such as Probability of Detection (POD), False Alarm Rate (FAR), Threat Score (TS), and
 468 Equitable Threat Score (ETS). Specifically, the average TS score of the CNN-BiLSTM-AM model for
 469 heavy precipitation reaches 0.336, representing a 33.2% improvement compared to the meteorologists'
 470 score of 0.252. Additionally, due to its training with a large-scale sample dataset, the model can
 471 automatically extract classification features and consider various parameters related to severe convective
 472 weather conditions. This enables it to assess the convective conditions at each grid point within the



473 forecast range, resulting in a lower miss rate than false alarm rate. This lower miss rate provides better
474 guidance for meteorologists' forecasts.

475 3) Using the RF algorithm, we perform an importance analysis of forecast factors on the training and
476 testing datasets of the CNN-BiLSTM-AM model, obtaining the relative rankings and correlation
477 coefficients of each forecast factor. The analysis results reveal that for severe convective weather,
478 precipitable water (PWAT) is the most critical moisture condition, with its importance significantly
479 surpassing the second-ranked feature. Geographic location also has a significant impact, with longitude
480 (LON) and latitude (LAT) ranking second and third among all factors, respectively. As convective
481 weather fundamentally arises from temperature variations, temperature (T) ranks fourth. Strong
482 convection imposes certain requirements on atmospheric dynamic lifting conditions, with 300hPa
483 vertical motion (W300) ranking fifth. Atmospheric energy conditions have some influence on severe
484 convective weather but are not the most important factors, as Bulk Convective Available Potential
485 Energy (BCAPE) and Lifted Index (LI) rank sixth and seventh, respectively. Through this ranking
486 analysis of forecast factors, we find that the order of importance determined by deep learning for severe
487 convective weather prediction is roughly consistent with the subjective understanding of meteorologists.
488 This further demonstrates the effectiveness of deep learning in automatically extracting features for
489 severe convective weather and verifies the rationality of constructing the sample dataset.

490



491 **Code availability**

492 The code and model are available at Zenodo via [https://doi.org/ 10.5281/zenodo.8417134](https://doi.org/10.5281/zenodo.8417134) (Zhang et al.,
493 2023).

494 **Data Availability**

495 The data are available at Zenodo via [https://doi.org/ 10.5281/zenodo.8417134](https://doi.org/10.5281/zenodo.8417134) (Zhang et al., 2023).

496

497 **Author contributions**

498 YY and ZG were responsible for conceptualization, supervision and funding acquisition. SZ developed
499 the software and prepared the original draft. SZ and YY developed the methodology and carried out
500 formal analysis. XX and SZ validated data. ZG, YY, XX, ZD, and YL were reviewed and edited the text.
501 SZ was responsible for visualization. All authors have read and agreed to the published version of the
502 paper.

503 **Competing interests**

504 The authors declare that they have no conflict of interest.

505 **Financial support**

506 This research has been supported by the second batch of service public bidding projects for EHV
507 transmission companies in 2022 (2022-FW-2-ZB) (grant no. CG0100022001526556).

508

509

510



511 **References**

- 512 Bi, K., Xie, L., Zhang, H., Chen, X., Gu, X., and Tian, Q.: Accurate medium-range global weather
513 forecasting with 3D neural networks, *Nature*, <https://doi.org/10.1038/s41586-023-06185-3>, 2023.
- 514 Buda, M., Maki, A., and Mazurowski, M. A.: Systematic study of the class imbalance problem in
515 convolutional neural networks, arXiv preprint arXiv:1710.05381, 2017.
- 516 Zeng, Y. and Yang, L. M.: Analysis on Mesoscale Impact System and Atmospheric Vertical Structure
517 of Two Types of Heavy Rains in Urumqi. *Plateau Meteorology*, 39, 774-787, [https://doi.org/10.7522/
518 j.issn.1000-0534.2019.00070](https://doi.org/10.7522/j.issn.1000-0534.2019.00070), 2020.
- 519 Gao, Z., Zhang, J., Yu, M., Liu, Z., Yin, R., Zhou, S., Zong, L., Ning, G., Xu, X., Guo, Y., Wei H., and
520 Yang, Y.: Role of water vapor modulation from multiple pathways in the occurrence of a record-
521 breaking heavy rainfall event in China in 2021, *Earth and Space Science*, 9, e2022EA002357,
522 <https://doi.org/10.1029/2022EA002357>, 2022.
- 523 Gope, S., Sarkar, S., Mitra, P., and Ghosh, S.: Early Prediction of Extreme Rainfall Events: A Deep
524 Learning Approach[M]// *Advances in Data Mining*, Springer International Publishing, 2016.
- 525 Han, H., Lee, S., Im, J., Kim, M., Lee, M., Ahn, M., and Chung, S.: Detection of Convective Initiation
526 Using Meteorological Imager Onboard Communication, Ocean, and Meteorological Satellite Based on
527 Machine Learning Approaches, *Remote Sens*, 7(7):9184-9204, <https://doi.org/10.3390/rs70709184>,
528 2015.
- 529 Herman, G. R. and Schumacher, R. S.: Money Doesn't Grow on Trees, but Forecasts Do: Forecasting
530 Extreme Precipitation with Random Forests, *Mon Wea Rev*, 146 (5):1571-1600,
531 <https://doi.org/10.1175/MWR-D-17-0250.1>, 2018.
- 532 Kingma, D. and Ba, J. A.: A Method for Stochastic Optimization, *Int Conf Learn Represent*,
533 <https://doi.org/10.48550/arXiv.1412.6980>, 2014.
- 534 Krawczyk, B.: Learning from imbalanced data: open challenges and future directions, *Progr Artif Intell*,
535 5(4):1-12, <https://doi.org/10.1007/s13748-016-0094-0>, 2016.
- 536 Krizhevsky, A., Sutskever, I., and Hinton, G. E.: Imagenet classification with deep convolutional neural
537 networks[C]// *Proceedings of the 25th International Conference on neural information processing*
538 *systems*, Red Hook, NY, United States: Curran Associates Inc: 1097-1105, 2012.



539 LeCun, Y. and Bengio, Y.: Convolutional networks for images, speech, and time series[M] //Arbib M A.
540 The handbook of brain theory and neural networks, Cambridge: MIT Press: 255-258, 2019.

541 Lin, T. Y., Li, Q. Y., Geng, Y. A., and Jiang, L.: Attention-Based Dual-Source Spatiotemporal Neural
542 Network for Lightning Forecast, IEEE Access, (7): 158296-158307, [https://doi.org/10.1109/ACCESS.](https://doi.org/10.1109/ACCESS.2019.2950328)
543 2019. 2950328, 2019.

544 Liu, N. N., Liu, C. T., and Tissot, P. E.: A Bayesian-Like Approach to Describe the Regional Variation
545 of High - Flash Rate Thunderstorms From Thermodynamic and Kinematic Environment Variables,
546 Geophys Res: Atmos,124(23): 12507-12522, <https://doi.org/10.1029/2019JD031254>, 2019.

547 Li, W. J., Zhao, F., Li, M. J., Chen, L., and Peng, X.: Forecasting and Classification of Severe Convective
548 Weather Based on Numerical Forecast and Random Forest Algorithm, Meteor Mon, 44(12):49-58(in
549 Chinese), <https://doi.org/10.7519/j.issn.1000-0526.2018.12.005>, 2018.

550 Lu, W. J., Li, J. Z., Wang, J. Y., and Qin, L.: A CNN-BiLSTM-AM method for stock price predictiona,
551 Neural Computing and Applications,33:4741–4753, <https://doi.org/10.1007/s00521-020-05532-z>, 2021.

552 McGovern, A., Elmore, K. L., Gagne II, D. J., Haupt, S. E., Karstens, C. D., Lagerquist, R., Smith, T.,
553 and Williams, J. K.: Using artificial intelligence to improve real-time decision-making for high-impact
554 weather, Bul Amer Meteor Soc, 98(10): 2073-2090, <https://doi.org/10.1175/BAMS-D-16-0123.1>, 2017.

555 McGovern, A., Lagerquist, R., Gagne II, D. J., Jergensen, G. ,E., Elmore, K. L., Homeyer, C. R., and
556 Smith, T.: Making the black box more transparent: Understanding the physical implications of machine
557 learning, Bull Amer Meteor Soc,100(11): 2175-2199, <https://doi.org/10.1175/BAMS-D-18-0195.1>,
558 2019.

559 Perol, T., Gharbi, M. and Denolle, M.: Convolutional Neural Network for Earthquake Detection and
560 Location, Sci Adv, (4):2–10, <https://doi.org/10.1126/sciadv.1700578>, 2017.

561 Reichstein, M., Camps-Valls, G., Stevens, B., Jung, M., Denzler, J., Carvalhais, N., and Prabhat.: Deep
562 learning and process understanding for data-driven Earth system science, Nature, 566(7743): 195-204,
563 <https://doi.org/10.1038/s41586-019-0912-1>, 2019.

564 Szegedy, C. and Toshev, A., Erhan D.: Deep neural networks for object detection[C]// Proceedings of
565 the 26th International Conference on Neural Information Processing Systems, Red Hook, NY, United
566 States: Curran Associates Inc.2013: 2553-2561, 2013.



567 Tang, W., Zhou, Q., Liu, X., Zhu, W., Mao, X.: Analysis on Verification of National Severe Convective
568 Weather Categorical Forecasts, *Meteor Mon*, 43(1):67-76(in Chinese), [https://doi.org/](https://doi.org/10.7519/j.issn.1000-0526.2017.01.007)
569 10.7519/j.issn.1000-0526.2017.01.007, 2017.

570 Tian, F., Zheng, Y., Zhang, T., Zhang, X., Mao, D., Sun, J., and Zhao, S.: Statistical characteristics of
571 environmental parameters for warm season short-duration heavy rainfall over central and eastern China,
572 *Meteor Res*, (29): 370-384, <https://doi.org/10.1007/s13351-014-4119-y>, 2015.

573 Wang, X., Mao, W., Guo, J.: Statistics features of strong convection weather disaster in China in 2004
574 main flood period, *J Nat Disasters*, 16(1): 27-30(in Chinese), 2007.

575 Zhang, F., Li, G., Luo, X.: Some Influence Factors of a Sudden Rainstorm Event in Northeast Sichuan
576 Basin of China, *Plateau Meteorology*, 39 (2) : 321-332, [https://doi.org/10.7522/j.issn.1000-](https://doi.org/10.7522/j.issn.1000-0534.2019.00080)
577 0534.2019.00080, 2020.

578 Zhang, J., Gao, Z., Yang, J., Li, Y., and Jiang, Y.: Research and Numerical Simulation of Rainstorm
579 over Bosten Lake Area based on WRF Model, *Plateau Meteorology*, 41 (4) : 887-895.
580 <https://doi.org/10.7522/j.issn.1000-0534.2021.00029>, 2022.

581 Zheng, Y., Tian, F., Meng, Z., Xue, M., Yao, D., Bai, L., Zhou, X., Mao, X., and Wang M.: Survey and
582 Multi Scale Characteristics of Wind Damage Caused by Convective Storms in the Surrounding Area of
583 the Capsizing Accident of Cruise Ship “Dongfangzhixing”, *Meteor Mon*,42(1):1-13(in Chinese),
584 <https://doi.org/10.7519/j.issn.1000-0526.2016.01.001>, 2016.

585 Zheng, Y., Zhou, K., Sheng, J., Lin, Y., Tian, F., Tang, W., Lan Y., and Zhu, W.: Advances in Techniques
586 of Monitoring, Forecasting and Warning of Severe Convective Weather, *J Appl Meteor Sci*, 26(6): 641-
587 657(in Chinese), <https://doi.org/10.11898/1001-7313.20150601>, 2015.

588 Zheng, Y., Zhu, W., Yao, D., Meng, Z., Xue, M., Zhao, K., Wu, Z., Wang, X., Zheng, Y.: Wind Speed
589 Scales and Rating of the Intensity of the 23 June 2016 Tornado in Funing County, Jiangsu
590 Province[J].*Meteor Mon*,42(11):1289-1303(in Chinese), [https://doi.org/10.7519/j.issn.1000-0526.2016.](https://doi.org/10.7519/j.issn.1000-0526.2016.11.001)
591 11.001, 2016.